ACS OMEGA

http://pubs.acs.org/journal/acsodf

Article

# Biodiesel Production from Waste Cooking Oil Catalyzed by a Bifunctional Catalyst

Vania Enguilo Gonzaga, Rubi Romero,* Rosa María Gómez-Espinosa, Amaya Romero, Sandra Luz Martínez, and Reyna Natividad*

Cite This: *ACS Omega* 2021, 6, 24092−24105

Read Online

ACCESS | Metrics & More | Article Recommendations

**ABSTRACT:** The objective of this study was to prepare bifunctional catalysts based on iron and CaO and test them in the biodiesel production using waste cooking oil (WCO) as feedstock. Two iron precursors were studied, $Fe_2O_3$ and $Fe(NO_3)_3{\cdot}9H_2O$. The identified crystalline phases were $Ca_2Fe_2O_5$ and $CaFeO_3$. Surface morphology and textural properties (distribution of active species, specific surface area, size, and pore volume) were also analyzed. Additionally, thermal stability was studied and 800 °C was established as the optimum calcination temperature. The density of both acidic and basic sites was higher with the catalyst prepared with $Fe_2O_3$ than with that prepared with $Fe(NO_3)_3{\cdot}9H_2O$. The latter, however, leads to reach equilibrium in half of the time than with the former. This was ascribed to the ratio of acidic to basic sites, which is higher with the catalyst prepared with the precursor salt. This ratio not only affects the overall cost of the process by affecting the time at which equilibrium is reached but also by dictating the methanol/oil molar ratio at which the equilibrium is reached sooner. The prepared bifunctional catalyst allowed us to produce biodiesel with 90% of methyl ester content at atmospheric pressure, reaction temperature of 60 °C, reaction time of 2 h, with 12:1 M ratio of methanol/WCO, 10 wt % of Fe over CaO, and a catalyst loading of 5 wt %. This catalyst can be used at least 3 times. The so-obtained biodiesel met the European norm EN-14214 regarding viscosity and density.

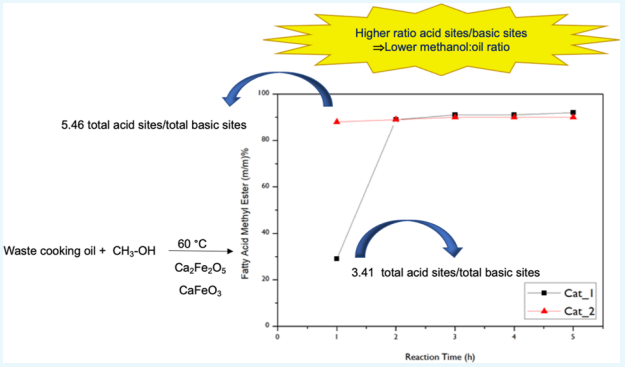




## 1. INTRODUCTION

New sustainable energy alternatives have emerged to replace the enormous dependence of society on limited fossil resources.[1,2] In this context, biodiesel is a viable alternative. Biodiesel is a form of biofuel used as a substitute for fossil diesel that can be used in diesel engines without conducting major modifications. Some advantages of biodiesel over fossil diesel include improved combustion efficiency, reduced carbon monoxide and hydrocarbon emissions, and increased lubrication capacity and oxygen content. Also, biodiesel is a renewable and biodegradable fuel.[3,4] The American Society for Testing and Materials defines biodiesel as a "fuel comprised of monoalkyl esters of long chain fatty acids derived from vegetable oils or animal fats". Usually, biodiesel is obtained by transesterification of refined oils or reused oils using basic or acidic catalysts in the presence of short-chain alcohols such as methanol or ethanol. Such catalysts can be homogeneous or heterogeneous.

One of the main advantages of heterogeneous catalysts over homogeneous catalysts is the easy separation and purification of biodiesel at the end of the reaction, minimizing the demand of washing water.[5,6] A disadvantage of basic heterogeneous catalysts is that they require oils with a low content of free fatty acids (FFAs). This implies the use of refined oils, and thus, the process becomes not competitive from an economic point of view.[7,8] In this sense, reused oils, such as waste cooking oil (WCO), represent a viable alternative to lower production costs; however, they have a high content of FFAs and can form an important amount of waxes and soaps.[7,8] To overcome this problem, esterification with acidic catalysts is carried out before transesterification. This alternative, however, involves several expensive and complex processes.

In the last decade, research on the synthesis of heterogeneous bifunctional catalysts has been reinforced to obtain biodiesel from raw materials with a high content of FFAs. Such bifunctional catalysts have acidic and basic centers that allow the esterification of FFA and transesterification of

**Received:** July 7, 2021
**Published:** September 10, 2021

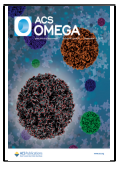

Table 1. Summary of the Literature Related to Biodiesel Production Catalyzed with Bifunctional Catalysts

| | | reaction conditions | | | | | |
|---|---|---|---|---|---|---|---|
| catalyst | feedstock | $T$ [°C] | methanol/oil ratio | catalyst weight [% wt] | reaction time [h] | methyl ester content [%] | refs |
| $MgO/Fe_2O_3-SiO_2$ | camelina oil | 70 | 12:1 | 4.9 | 4.1 | 99 | 12 |
| $\alpha$-$Fe_2O_3$/AlOOH | cottonseed waste oil | 60 | 6:1 | 3 | 3 | 95 | 13 |
| $\alpha$-$Fe_2O_3$/AlOOH($\gamma$-$Al_2O_3$) | cottonseed waste oil | 60 | 6:1 | 3 | 3 | 94.3 | 14 |
| $CaSO_4/Fe_2O_3-SiO_2$ | crude *Jatropha curcas* oil | 120 | 9:1 | 12 | 4 | 94 | 15 |
| $Fe_2O_3$/CaO | used frying oil | 65 | 15:1 | 1 | 3 | 92 | 1 |
| Na/NaOH/$Al_2O_3$ | soybean oil | 60 | 20:1 | 5 | 2 | 100 | 16 |
| CaO/$La_2O_3$ | crude *Jatropha curcas* oil | 160 | 25:1 | 3 | 3 | 98.76 | 17 |
| CAWS-$_{(7)}SO_4$ | PFAD (palm fatty acid distillate) | 80 | 15:1 | 5 | 3 | 98 | 18 |
| CaO/$\gamma$-$Al_2O_3$ | edible refined sunflower oil | 60 | 9:1 | 0.55 | 5.22 | 97.8 | 19 |
| $W_XMo_Y$/CaO | PDWO (unrefined palm-derived waste oil) | 70 | 15:1 | 2 | 2 | 96.2 | 20 |
| $CaFe_2O_4/Ca_2Fe_2O_5$ | soybean oil and *Jatropha curcas* oil | 100 | 15:1 | 4 | 2 | 85.4 | 21 |
| CaO/SA (22.4)-FS | olive pomace oil | 62 | 6:1 | 2 | 4 | 96.01 | 22 |
| 4Mn−6Zr/CaO | waste cooking oil | 80 | 15:1 | 3 | 3 | 92.1 | 23 |
| $Fe_3O_4$/CaO | palm oil off-grade | 70 | 10:1 | 1 | 2 | 90 | 24 |
| cellulose/CaO−$Fe_2O_3$ | coconut oil | 60 | 12:1 | 3.6 | 5 | 89.2 | 25 |
| Mo−Zr/CS | waste cooking palm oil | 80 | 15:1 | 3 | 3 | 90.1 | 26 |
| CaO@$\gamma$-$Fe_2O_3$ | dehydrated soybean oil | 70 | 15:1 | 2 | 3 | 98.8 | 27 |

triglycerides to be carried out in a single stage.[9,10] This makes them attractive at an industrial level since their use would reduce production costs. Bifunctional catalysts are a mixture of metal oxides, whose characteristics depend on the preparation method and the metals used. In this sense, bifunctional catalysts based on CaO have demonstrated to be a promising alternative. In Table 1, there are the summarized CaO-based bifunctional catalysts that were selected according to the relevance of their performance in biodiesel production.

It can be seen in Table 1 that the doping of CaO is a proven strategy to obtain high methyl ester content (>90%) either from refined or waste oils. Regarding the latter, it has also been reported that doping the CaO reduces its deactivation.[11] The methyl ester content is an indicator of the biodiesel quality and depends mainly on the operational variables included in Table 1. According to the works shown in Table 1, a high methyl ester content is attained, in some cases, at temperatures rather high (160 °C) and alcohol/oil molar ratios as high as 25:1 and with reaction times that vary between 2 and 5.5 h. By conducting an analysis of the results reported in the references included in Table 1, it can be concluded that the addition of metal oxides affects the acidic site density, which in turn has been related in some works to the methyl ester content mainly when the FFA content is high such as in the case of waste oils (FFA > 1%).

Among the preferred metals to modify the acidic site density, one can find Fe, Mo, W, and Zr. It can also be observed in the available literature that, generally speaking, doping of CaO with iron oxides not only impacts the acidic site density but also allows us to obtain methyl esters at moderate reaction temperature. Only relatively few works can be found regarding the production of biodiesel using iron oxides and CaO as bifunctional catalysts. Furthermore, in most of these works, the bifunctional catalyst is underutilized since it is applied to catalyze the biodiesel production from refined oils that usually exhibit a relatively low acid value. In the context of iron and calcium bifunctional catalysts, the activity of the catalyst has been mainly related to the iron oxide structure, such as $Fe_3O_4$, $Fe_2O_3$, $\gamma$-$Fe_2O_3$, $CaFe_2O_4$, and $Ca_2Fe_2O_5$, and to the basic site density. In only few works, the importance of the acidic site density has been hinted, and other works with catalysts, such as W−Zr/CaO, have stated that both acidic and basic sites are important. None of these works, however, pay attention to the ratio of acidic to basic sites and its relationship with the iron precursor, FAME (fatty acid methyl ester) content and methanol/oil molar ratio. Therefore, the main objective of this work was to prepare a bifunctional catalyst (based on iron over calcium oxide) for FAME production using WCO and to evaluate the influence of its properties (morphological, textural, structural, and chemical) on FAME content. From an economic point of view, it is rather important to establish the catalyst properties and preparation conditions that might lower the cost of the overall process. In this sense, it is worth pointing out that quicklime was used as the source of CaO. Furthermore, one of the investigated variables is the precursor of the iron. Two iron precursors are compared, $Fe_2O_3$ and $Fe(NO_3)_3{\cdot}9H_2O$, the cost of the former being lower than the latter. The precursor salt, however, is typically utilized in the related literature.[1,21,25,27]

## 2. EXPERIMENTAL METHODS

**2.1. Materials.** WCO was provided by a local food industry. Quicklime, a source of CaO, was acquired from a local store. The fatty acid composition of WCO is shown in Table 2.

The acid value, density, viscosity, and water content were obtained according to quality methods (Norm EN-14214). These results are shown in Table 3. Methanol ACS ($CH_3OH$) 99.9% was supplied by Fermont. Iron(III) nitrate ($Fe(NO_3)_3{\cdot}9H_2O$) 99.0% was bought from Merck, and iron(III) oxide ($Fe_2O_3$) 99.0% was obtained from Reasol. In order to quantify the FAMEs by gas chromatography, the reference standard (methyl heptadecanoate, >99.7%) was purchased from Sigma Aldrich and *n*-heptane high-performance liquid chromatography $CH_3(CH_2)_6CH_3$ from J.T Baker.

**2.2. Pretreatment of WCO.** The WCO required a pretreatment to remove solid particles, soluble salts, and moisture. Initially, to eliminate the solid particles, the used



https://doi.org/10.1021/acsomega.1c03586
ACS Omega 2021, 6, 24092−24105

Table 2. Fatty Acid Composition of WCO

| fatty acid composition | % |
|---|---|
| lauric (C12:0) | 0.03 |
| myristic (C14:0) | 0.16 |
| palmitic (C16:0) | 12.03 |
| palmitoleic (C16:1) | 0.17 |
| margaric (C17:0) | 0.12 |
| stearic (C18:0) | 4.40 |
| oleic (C18:1) | 23.58 |
| linoleic (C18:2) | 52.48 |
| arachidic (C20:0) | 0.33 |
| linolenic (C18:3) | 6.65 |

Table 3. WCO Properties

| property | value |
|---|---|
| acid value (mg KOH/g) | 2.53 |
| free fatty acid (wt %) | 1.26 |
| molecular weight (g/mol) | 277.84 |
| water content (wt %) | 0.042 |
| density at 15 °C (kg/m$^3$) | 926.02 |
| viscosity at 40 °C (mm$^2$/s) | 36.08 |

cooking oil was filtered. After that, a process with hot water was carried out to remove gums. This process consisted of the addition of water at 80 °C to the previously heated oil. Finally, the oil was separated and kept under vacuum at 80 °C to eliminate the excess of moisture.

**2.3. Catalyst Synthesis.** First, lumps of quicklime were triturated to obtain particles of a homogeneous size of 0.42 mm. To transform $Ca(OH)_2$ (major component of quicklime) to CaO, a heat treatment in a furnace was necessary. The conditions of calcination were 900 °C with a ramp of 2 °C/min for 8 h.[28]

Bifunctional catalysts based on iron(III) and CaO were prepared by an ion exchange method. This method has also been used by Ezzah-Mahmudah et al.,[1] albeit without assessing the effect of the iron precursor or the iron oxide structure (calcination temperature) and with additional preparation stages (washing of the catalyst with distilled water after filtration).

In this work, the effect of the iron(III) precursor was investigated by using either $Fe_2O_3$ (Cat_1) or $Fe(NO_3)_3 \cdot 9H_2O$ (Cat_2). This variable was studied with a 10 wt % iron catalyst (Fe/Ca mass ratio = 0.15). This percentage was selected since compared to the other assessed iron contents (1, 2.5, and 5 wt %), it provided the best results in terms of FAME content and time to reach equilibrium. To prepare the catalyst with 10 wt % of iron, 3.6 g of CaO was dispersed in 400 mL of water, and then, the mixture was stirred for 5 min. Next, 0.54 g of $Fe_2O_3$ or 2.86 g of $Fe(NO_3)_3 \cdot 9H_2O$ was slowly added to the slurry in such a way that a $1.79 \times 10^{-2}$ M concentration of iron(III) could be attained. The resulting mixture was stirred for 4 h. Next, the suspension was filtered and the solid was dried overnight at 100 °C. The effect of the calcination temperature was studied by calcining the material at 500 and 800 °C for 5 h. This variable was also assessed with 10 wt % of iron over the CaO catalyst.

The study of the variables was conducted under the following reaction conditions: 60 °C of temperature, reaction time of 5 h with 12:1 methanol/oil ratio, and 5 wt % of catalyst loading.

**2.4. Catalyst Characterization.** The crystalline phases of bifunctional catalysts were analyzed by X-ray diffraction in a PHILIPS PW-1711 diffractometer with Cu K$\alpha$ radiation at 30 kV and 25 mA. The samples were scanned in the 2$\theta$ range from 20 to 100° and step time of 0.04°.

The surface morphology and distribution of the active species of the bifunctional catalysts were analyzed in a JEOL JSM-6510LV scanning electron microscope coupled with an energy-dispersive X-ray spectrometer.

The specific surface area, size, and pore volume of the bifunctional catalysts were determined by $N_2$ adsorption and desorption data acquired with a Quadrasorb SI surface area and pore size analyzer. Prior to adsorption, the samples were degassed under high vacuum (1013 mbar) for 4 h and 180 °C and 1 h under vacuum ($10^{-7}$ mbar) at 180 °C.

The thermal stability of the catalyst was examined in a SDT Q600 simultaneous TGA/DSC apparatus under a purge flow of 30 mL/min of nitrogen and within a temperature range of 25−1000 °C with a heating rate of 10 °C/min.

A temperature-programmed reduction (TPR) study was carried out in an AutoChem 2950 HP chemisorption analyzer. First, the sample was treated with argon flow at 20 cm$^3$/min and 250 °C for 10 min. Subsequently, a mixture of gases (5% $H_2$-95% Ar) was passed at 40 cm$^3$/min through the sample for 30 min. During heating at 10 °C/min, the temperature and detector signals were recorded. The determination of $H_2$ consumption was carried out using a thermal conductivity detector (TCD).

Total basic and acidic site density, as well as strength distribution of the bifunctional catalysts, were measured by temperature-programmed desorption (TPD-$CO_2$ and TPD-$NH_3$). The apparatus used was the same as the one described above. The samples were heated at 5 °C/min up to 50 °C under a flow of helium (100 cm$^3$/min). After a period of 30 min at this temperature, a stream of $CO_2$ was allowed to flow over the sample. To eliminate physisorbed species, a flow of helium (100 cm$^3$/min) was passed through the sample for 1 h. $CO_2$ desorption of the samples was recorded using a TCD at 900 °C with a ramp of 10 °C/min. Acidity analysis was carried out under the same conditions, only that in this case, the used gas was ammonia ($NH_3$).

The percentage of metals in the catalysts was determined in a Varian Liberty RL sequential ICP-AES multielemental analyzer. Prior to analysis, the solid samples were subjected to acid digestion treatment with concentrated nitric acid (5 mL) and concentrated hydrochloric acid (5 mL) to achieve the dissolution of metals.

**2.5. Biodiesel Production.** The synthesized catalysts were tested in the biodiesel production using WCO as the raw material. First, however, in order to demonstrate the advantage of adding iron to CaO, an experiment with only CaO (calcined quicklime) was conducted. The reaction conditions for this experiment were: methanol/oil molar ratio = 12:1, reaction temperature = 60 °C, and 5 wt % of CaO. Unless otherwise stated, these conditions were also used to establish the effect of the other variables: the amount of the catalyst (with 10% of iron) with respect to the mass of oil (1, 3, 5, and 7%), percentage of iron supported on CaO (0, 1, 2.5, 5, and 10 wt %), methanol/oil molar ratio (9:1, 12:1, 18:1, and 25:1) with the catalyst with 10% of iron, and reaction time (1−5 h). The range of study of the molar methanol/oil was established based on the previous literature related to the processing of WCO with doped CaO.[1,20,24,26] The reaction temperature was kept


https://doi.org/10.1021/acsomega.1c03586
ACS Omega 2021, 6, 24092−24105

constant in all experiments. These were conducted in a glass stirred tank reactor (250 mL) with baffles. The temperature was constantly monitored with a thermometer. A methanol reflux system was placed on top of the reactor. This system consisted of a condenser that was being constantly cooled by recirculating an antifreeze coolant through the condenser. The stirring was conducted with a magnetic bar and the heating with a thermal plate. Once the methanol−catalyst mixture was heated at 60 °C, the WCO, also at the same temperature, was added and mixed at approximately 600 rpm. The reaction was monitored for 5 h, taking a sample every hour. To recover the catalyst at the bottom, the samples were centrifuged at 3500 rpm, and then, methanol was separated via evaporation and glycerol was recovered by settling.

**2.6. Biodiesel Characterization.** The FAME content was determined using a SCION model 456 gas chromatograph with a flame ionization detector and HP-INNOWAX polar capillary column (30 m length, 0.320 mm internal diameter, and 0.25 $\mu$m film). This quantification was conducted according to the European regulation procedure UNE-EN14103. The kinematic viscosity at 40 °C was determined using a Canon-Fenske capillary viscometer following the European Norm EN ISO 3104. Finally, density was measured in an Anton Paar densimeter model DMA 5000 M. Both the reactions and the analysis of FAMEs by chromatography were performed 3 times. The calculated error was 3%.

**2.7. Catalyst Stability.** The stability of the bifunctional catalyst was tested by evaluating the reusability. For this purpose, the bifunctional catalysts were used in consecutive transesterification reactions to verify their catalytic performance. For these experiments, the used solid catalyst was separated from the reaction mixture by centrifugation. After that, the catalyst was washed with hexane to remove nonpolar compounds, such as methyl esters, and then washed with methanol to eliminate polar compounds, for example, glycerol. Finally, the catalyst was dried at 100 °C for 12 h and activated at 800 °C for 4 h; the active used catalyst was directly used in repeated reactions under the best resulting conditions of this study (temperature 60 °C, 5 wt % catalyst, and 10 wt % of iron over CaO using iron nitrate as the precursor).

## 3. RESULTS AND DISCUSSION

**3.1. Catalyst Characterization.** The crystalline phases of bifunctional catalysts and calcined quicklime were determined by X-ray diffraction. As can be seen in Figure 1, after calcination at 900 °C for 8 h, the principal components of quicklime [$Ca(OH)_2$ and $CaCO_3$] were completely transformed to CaO. Characteristic CaO peaks were obtained at 2$\theta$: 32.26, 37.46, 53.90, 64.18, and 67.44° (JCPDS # 75-0264). This result is consistent with that reported by Ezzah-Mahmudah et al.,[1] Camacho et al.,[28] and Nunes et al.,[29] who suggested that the optimal temperature to transform $CaCO_3$ and $Ca(OH)_2$ from oyster shells, quicklime, and egg shells to CaO is 900 °C. The X-ray diffraction patterns of bifunctional catalysts prepared from different precursors are also depicted in Figure 1 (Cat_1 and Cat_2). In such patterns, an increase in the crystallinity of the CaO structure was observed with respect to the calcined CaO. In addition, brownmillerite ($Ca_2Fe_2O_5$) was identified in both, Cat_1 and Cat_2, catalysts at 2$\theta$: 32.18, 33.5, 43.4, and 46.7°, with an orthorhombic crystalline system (JCPDS # 11-0675) at a small concentration. This compound is considered to be a mixed oxide

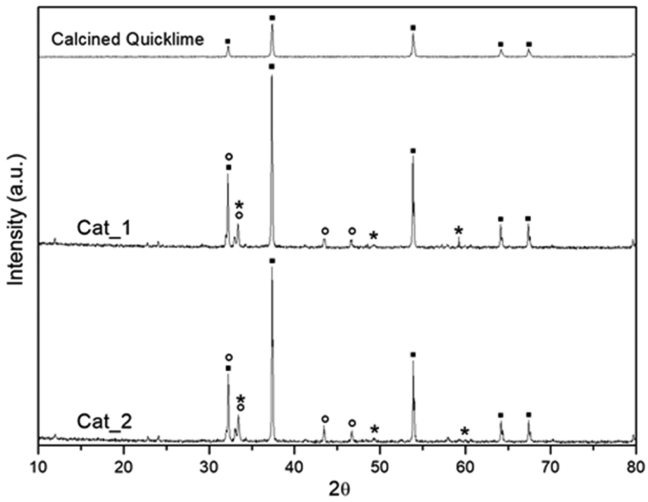


**Figure 1.** XRD patterns of calcined quicklime, Cat_1, and Cat_2 with a 10% w/w of iron [■CaO (JCPDS # 750264), ∘$Ca_2Fe_2O_5$ (JCPDS # 11-0675), and *$CaFeO_3$ (JCPDS # 41-0753)].

associated with the crystalline phase in which the iron has an oxidation state of $3^+$.[30]

As can be seen in Figure 1, the synthesized materials also showed the $CaFeO_3$ crystalline phase with a perovskite tetragonal crystal structure whose characteristic peaks of the species are found at 2$\theta$: 33.5, 48.5, and 60.04° (JCPDS # 41-0753). Finally, the absence of the $Fe_2O_3$ phase indicates an adequate distribution of the metal oxides over calcium oxide[31] and that in this case, this phase is not the one responsible for the catalytic activity of the synthesized materials.

Figure 2 is a representative scanning electron micrograph of the calcined quicklime and prepared bifunctional catalysts. Typical porous and amorphous morphology of calcium oxide can be observed for calcined quicklime; the calcined samples have irregular shapes, and pores are more visible; these characteristics are in concordance with previous studies.[32] When the iron(III) precursor was added to CaO, a change in morphology of the external surface was observed in Cat_1 and Cat_2, and the development of agglomerated structures was observed. This is probably due to the change in the crystalline phase, as indicated by XRD analysis. The agglomerates present different average sizes depending on the iron precursor, that is, 0.75 and 1.39 $\mu$m for Cat_1 and Cat_2, respectively. Also, both bifunctional catalysts exhibit a porous nature, and this is an important characteristic during transesterification and esterification reactions.

According to EDS chemical mapping (Figure 3), the bifunctional catalysts contain calcium and iron, homogeneously dispersed. Regarding iron, Figure 3 suggests that there is a higher Fe content in Cat_2 than in Cat_1. This is true despite being prepared based on the calculation of having the same final iron % w/w (10%). The amount of iron and calcium present in the catalysts was determined by inductively coupled plasma−atomic emission spectroscopy (ICP-AES) analysis. Although it was aimed to obtain 10 wt % of iron in each catalyst, it was determined that Cat_2 contained a higher amount of iron (10%) compared to Cat_1 (7.2%). This is probably due to the iron nitrate salt dissolving easily in the impregnating medium, thus allowing iron ions ($Fe^{3+}$) to diffuse more effectively through the CaO. Finally, the amount of


https://doi.org/10.1021/acsomega.1c03586
ACS Omega 2021, 6, 24092−24105

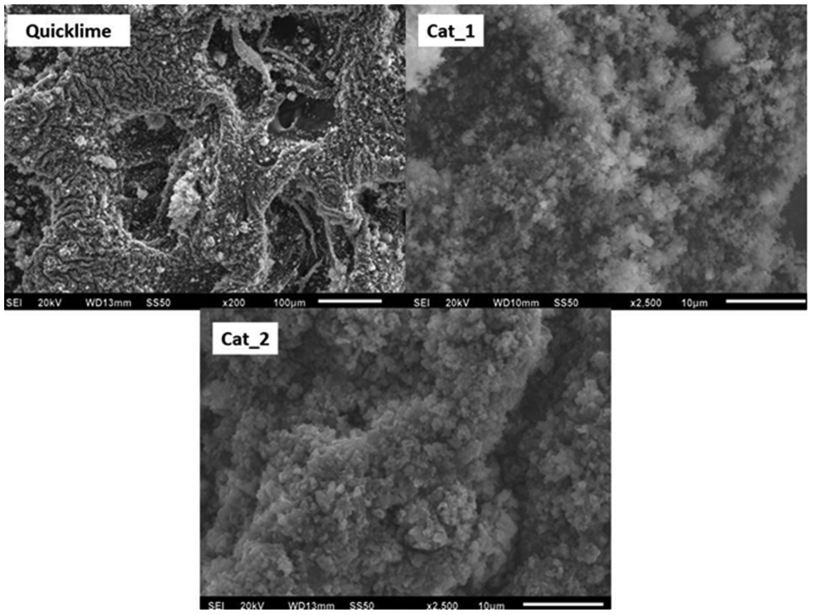


**Figure 2.** Scanning electron microscopy images of quicklime, Cat_1, and Cat_2 catalysts with 10 wt % of iron.

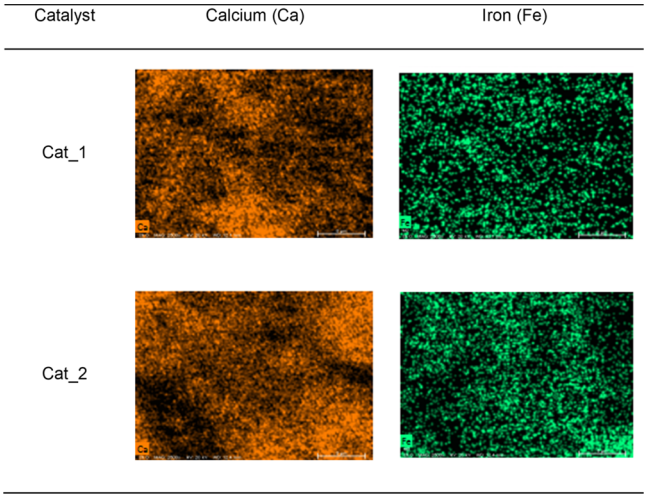


**Figure 3.** Chemical mapping of iron (10 wt %) and calcium in bifunctional catalysts.

calcium in both catalysts is similar, that is, 58.30 wt % for Cat_1 and 57.30 wt % for Cat_2.

The BET area, pore volume, and pore size of calcined quicklime (CaO) and bifunctional catalysts are shown in Table 4. The surface area of calcium oxide was 7.99 $m^2/g$. It has been reported that the incorporation of some dopants improves the surface area.[31,33] When ferric oxide was added to CaO (Cat_1), the area increased from 7.99 to 12.15 $m^2/g$. This effect is probably due to the strong interaction and adequate dispersion of iron with the support, reducing the surface diffusion of Ca; this hinders the sintering and stabilizes the crystal surface of CaO. This trend is in concordance with that reported by Wan Omar et al.,[34] who observed an increase in the surface area when doping zirconia with alkaline metals. Additionally, Rabiah Nizah et al.[33] reported that the addition of $Bi_2O_3$ over $La_2O_3$ also increases the surface area of the final material, and this was ascribed to the effective dispersion of dopants onto the support. Finally, Alhassan et al.[31] synthesized $Fe_2O_3$−MnO− $SO_4^{-2}/ZrO_2$ and determined that the disperse $Fe_2O_3$ over $ZrO_2$ surface avoids the agglomeration of metal oxides throughout the calcination process.

**Table 4. Textural Properties of Bare CaO and the Prepared Catalysts**

| catalysts | surface area ($m^2/g$) | pore volume ($cm^3/g$) | pore size (Å) |
|---|---|---|---|
| CaO | 7.99 | 0.0683 | 171.00 |
| Cat_1 | 12.15 | 0.0754 | 124.17 |
| Cat_2 | 6.71 | 0.0267 | 79.59 |

For Cat_2, when iron nitrate was used as the precursor, a different effect was observed. The surface area was reduced to 6.71 $m^2/g$. This effect might be attributed to the partial blockage of pores.[31] Also, previous studies concluded that the decomposition of iron precursors defines morphology and tends to reduce the surface area.[35] In addition, previous studies of bifunctional catalysts have reported similar surface characteristics for impregnated CaO.[17,36]

All the catalysts have a pore diameter greater than the average diameter of the triglyceride molecule (58 Å). It was observed, however, that the addition of iron causes a decrease in the average pore diameter size of CaO from 171 to 124.17 and 79.59 Å for Cat_1 and Cat_2, respectively. Thus, it can be observed that in the case of Cat_1, the average pore diameter is about twice the diameter of the triglyceride molecule, so the pores are large enough to allow reagents to pass through. In the case of Cat_2, however, the average pore diameter is closer to the size of the triglyceride molecule, and this might hinder or restrict diffusion. Finally, the prepared catalysts can be defined as mesoporous since the pore diameter was between 20 and 500 Å.

To establish the calcination temperature, quicklime and bifunctional catalysts were analyzed by thermogravimetric analysis (TGA) and the results are shown in Figure 4. As can be seen, quicklime lost weight in three steps. The first step at around 150 °C, can be attributed to the loss of physisorbed water on the catalyst surface. The second step, at around 400 °C, is due to the decomposition of calcium hydroxide


https://doi.org/10.1021/acsomega.1c03586
ACS Omega 2021, 6, 24092−24105

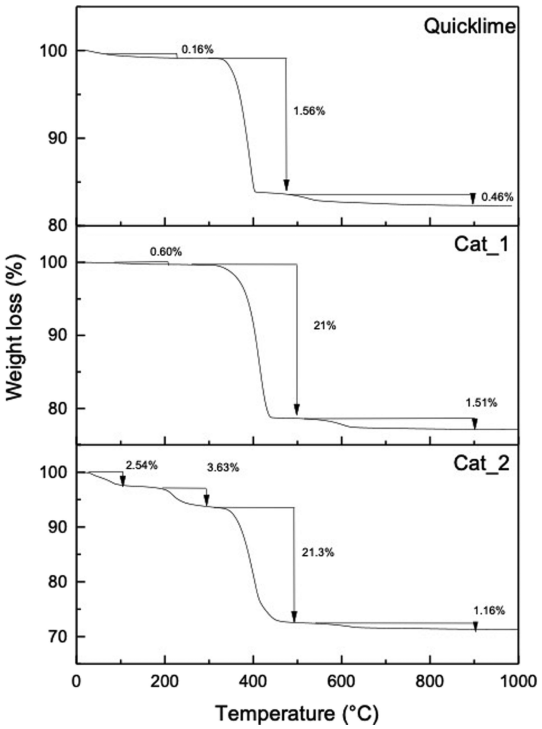


**Figure 4.** TGA analysis of quicklime, Cat_1, and Cat_2 catalysts with 10 wt % of iron.

($Ca(OH)_2$). This result agrees with that of Camacho et al.,[28] who reported the decomposition of calcium hydroxide at 380 °C. Finally, at 800 °C, the third loss of weight corresponds to the decomposition of calcium carbonate to calcium oxide. This result is in concordance with X-ray diffraction analysis, confirming that at 900 °C, only calcium oxide is present.

The TGA curve for Cat_1 shows three weight losses just like the TGA curve for quicklime. In this case, however, there are additional thermal transformations, one between 350 and 500 °C (stage 3c) and a second one between 550 and 900 °C (stage 4b). These transformations are summarized in Table 5. As can be seen, $CaFe_2O_4$ can be obtained at 500 °C, while $Ca_2Fe_2O_5$ can be obtained at any temperature between 550 and 900 °C.

**Table 5. Thermal Transformations of the Prepared Materials**[21,37,38]

| stage | temperature ranges | process |
|---|---|---|
| 1 | 50−100 °C | $H_2O\uparrow$ |
| 2 | 200−250 °C | $Fe(NO_3)_3{\cdot}9H_2O \rightarrow FeOOH + 3HNO_3 + 7H_2O$ |
| 3 | 350−500 °C | (a) $Ca(OH)_2 \rightarrow CaO + H_2O$ |
| | | (b) $FeOOH \rightarrow 1/2\ Fe_2O_3 + 1/2H_2O$ |
| | | (c) $CaO + Fe_2O_3 \rightarrow CaFe_2O_4$ |
| 4 | 550−900 °C | (a) $CaCO_3 \rightarrow CaO + CO_2$ |
| | | (b) $2CaO + Fe_2O_3 \rightarrow Ca_2Fe_2O_5$ |

Finally, Cat_2 showed four losses of weight. At 100 °C, the elimination of water is observed. At 200 °C, the decomposition of iron nitrate nonahydrate begins; when the temperature reaches 400 °C, there are two decompositions; the first one can be ascribed to the transformation of calcium hydroxide to calcium oxide, and the second one is due to the formation of iron(III) oxide. Finally, calcium oxide is obtained, derived from the decomposition of calcium carbonate. This is summarized in Table 5. These results are in agreement with Ezzah-Mahmudah et al.,[1] who studied the thermal transformations of iron nitrate over cockle shells.

TPR analysis of bifunctional catalysts allows us to obtain information of reducible species in the materials and the interaction force of iron with calcium.[39] Figure 5 shows the

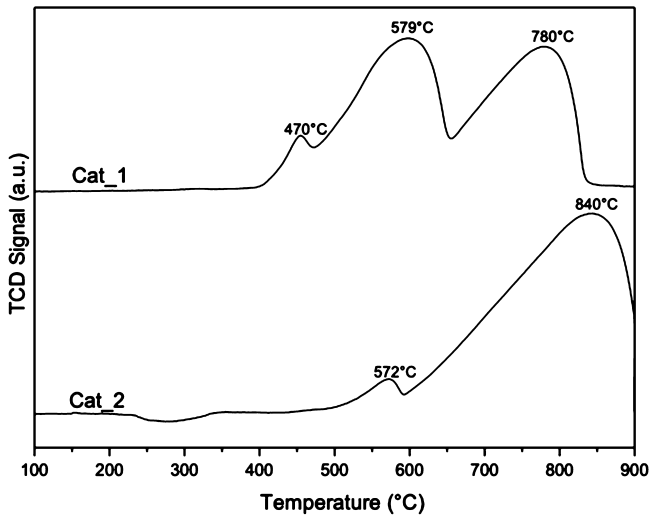


**Figure 5.** TPR profile of Cat_1 and Cat_1 with 10 wt % of iron.

TPR profiles of Cat_1 and Cat_2 with a theoretical 10% w/w of iron. Three peaks were identified for the Cat_1 catalyst. The first at 470 °C is attributed to the reduction of the $CaFeO_3$ species, detected by XRD. The second peak at 579 °C is due to the reduction of $Fe_3O_4$ to FeO. Finally, the peak at 780 °C can be ascribed to the reduction of $Ca_2Fe_2O_5$. The presence of three reduction peaks can be attributed to the low interaction of iron with the support.[35]

As can be seen in the TPR profile of the Cat_2 catalyst, only two reduction peaks were observed. A small peak at 572 °C can be attributed to calcium oxide reduction. A second one at 840 °C is due to the reduction of $Fe^{+3}$, present in the $Ca_2Fe_2O_5$ species, to $Fe^0$. The high reduction temperature demonstrates the stability of the bimetallic oxide in which iron interacts strongly with the support; these results are similar to those previously reported for the Fe/CaO interaction.[40]

Both basicity and acidity of bifunctional catalysts were determined using $CO_2$ and $NH_3$−TPD, respectively. The results are shown in Figure 6. As can be seen in TPD desorption, both catalysts exhibited bifunctional properties having acidic and basic sites.

TPD-$CO_2$ analysis for both catalysts showed two desorption peaks of $CO_2$; see Figure 6a,b. The first one, from 350 to 400 °C, can be attributed to the interaction of $CO_2$ with sites of medium basic strength. The second peak from 550 to 650 °C can be associated with strong basic strength. The amount of $CO_2$ desorbed of the Cat_1 catalyst was larger than that of the Cat_2 catalyst (Table 6), indicating greater basic strength. Strong basic sites correspond to the presence of CaO due to the isolated $O^{2-}$ anions situated in the mixed oxide surface.[34] The results are in good agreement with those previously reported.[41−43]

Meanwhile, the TPD-$NH_3$ analysis for both catalysts with a 10% w/w of iron also showed two desorption peaks; see Figure 6c,d. The first one appeared between 350 and 400 °C, while


https://doi.org/10.1021/acsomega.1c03586
ACS Omega 2021, 6, 24092−24105

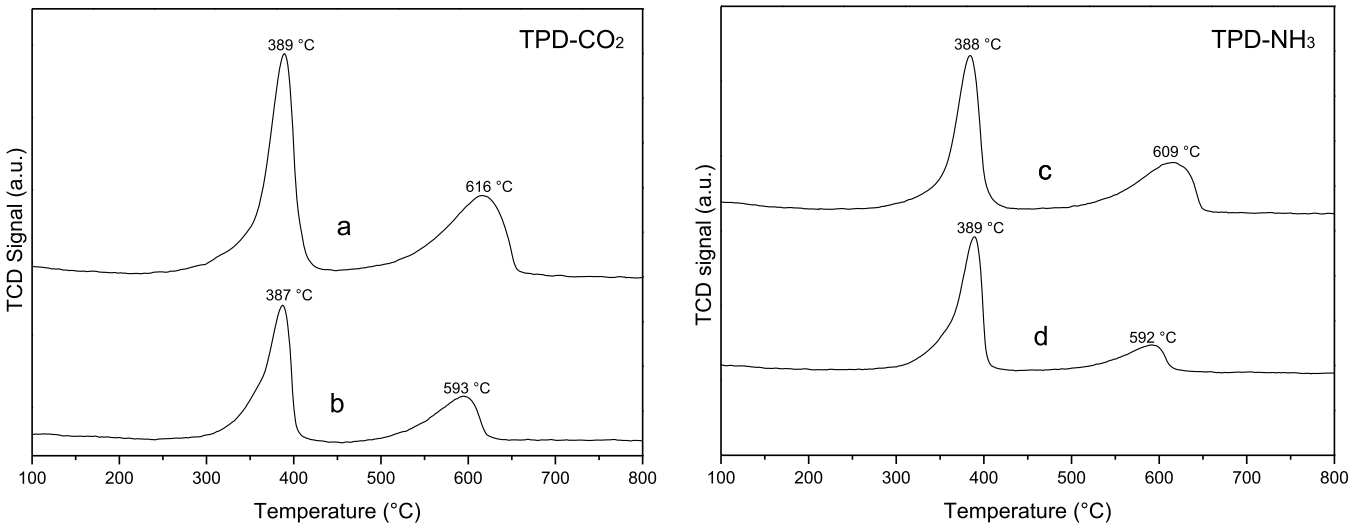


**Figure 6.** $CO_2$-TPD profiles for (a) Cat_1 and (b) Cat_2 and NH3-TPD profiles for (c) Cat_1 and (d) Cat_2 with 10 wt % of iron.

**Table 6. Density of Basic and Acidic Sites of Bifunctional Catalysts**

| | basic site density ($\mu$mol $CO_2$/g) | | acidic site density ($\mu$mol $NH_3$/g) | |
|---|---|---|---|---|
| catalyst | weak sites | strong sites | weak sites | strong sites |
| Cat_1 | 93.16 | 65.06 | 301.47 | 238.19 |
| Cat_2 | 42.37 | 22.86 | 241.27 | 115.38 |

the second one was detected in the range of 550−650 °C. These peaks were also attributed to medium and strong acid strength, respectively.[34] The temperatures of desorption and acidity were in good agreement with those reported by Alhassan et al.[44] who synthesized $Fe_2O_3$−MnO−$SO_4^{2-}$/$ZrO_2$ as a heterogeneous acid−base bifunctional catalyst.

In Table 6, the basic and acidic site density as well as basicity and acid strength attained with every catalyst are summarized. It can be observed that Cat_1 exhibits a higher basic and acidic site density than Cat_2. The same occurs with strength.

**3.2. FAME Production.** *3.2.1. Effect of Catalyst Calcination Temperature.* Table 7 shows FAME content

**Table 7. Effect of Calcination Temperature on FAME Percentage at Equilibrium**

| | calcination temperature | |
|---|---|---|
| catalysts | 500 °C | 800 °C |
| Cat_1 | 62%FAMEs | 91%FAMEs |
| Cat_2 | 67%FAMEs | 90%FAMEs |

related to the equilibrium state (3 h) for every catalyst calcined at different temperatures. It can be observed that less than 70% of the FAME content was obtained with the catalysts calcined at 500 °C. This may be due to the formation of CaO not being complete at this temperature.[28,45]

In addition, it has been demonstrated by Helwani et al.[24] that the effect of the calcination temperature is of paramount importance since it determines the strength of the produced basic sites. These researchers used $Fe_3O_4$ as the iron precursor and established that when calcining at 500 °C, the strength of the basic sites was lower than when calcining at 600 °C.

On the other hand, when the calcination temperature was increased to 800 °C, the FAME percentage increased significantly (Table 7). XRD analysis indicated that at 800 °C, only CaO and mixed iron oxides are present. In addition, the TGA analysis shows that at higher temperatures, there are no further transformations. Therefore, the calcination temperature of 800 °C was selected to study the effect of other variables.

*3.2.2. Effect of the Iron(III) Precursor.* It has been reported that the addition of metal oxides such as iron oxide(III) over some supports has significant chemical advantages such as improved catalyst thermal stability and generation of acidic sites.[1,44,46] Besides, it has been shown that the type of the iron(III) precursor largely defines the chemical and morphological properties of the synthesized catalyst.[35]

Figure 7 shows a different behavior at the initial reaction time for each catalyst. This trend reveals the different catalytic activity of each material. In the first hour of the reaction, the catalysts reached 29 and 88% of FAMEs for Cat_1 and Cat_2, respectively. For both catalysts, the maximum FAME % is reached within the first and the second hour of the reaction.

The different initial behavior can be ascribed to the acidic and basic characteristics of materials. In the context of the use of CaO doped with iron oxides, the works reported in Table 1[1,21,24,25,27] suggest that there is a relationship between the FAMEs obtained and the strength of the basic sites in the surface. This is true when the feedstock is a refined oil[21,27] but is controversial when the feedstock is a high-FFA-content oil[1,23,24] since the highest FAME % is not obtained with the catalyst with the strongest basic sites or with the highest concentration of them. It is with other CaO dopants, such as W−Zr[20] and Mn−Zr,[23] that the importance of the acidic sites has been evidenced, and therefore, it has been suggested that the final FAME content achieved with a bifunctional catalyst may depend on the equilibrium of acidic and basic sites available for reaction.[20,33,46] Nevertheless, this has not really been proven with CaO doped with iron species. In this sense, the results shown in Table 8 suggest that what really dictates the initial FAME production reaction rate catalyzed with a bifunctional catalyst is the ratio of acidic sites to basic sites rather than their density and strength. The final FAME content (at equilibrium) is not affected by this property although. However, it is worth pointing out that the production cost of


https://doi.org/10.1021/acsomega.1c03586
ACS Omega 2021, 6, 24092−24105

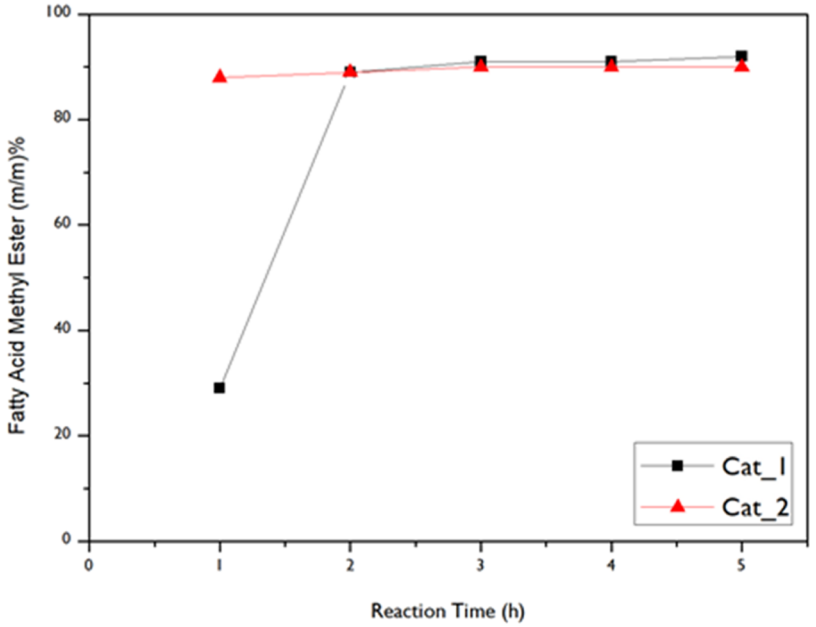


**Figure 7.** Effect of the iron(III) precursor on FAME profiles as a function of time. Reaction conditions: $T$ = 60 C, 12:1 methanol/oil molar ratio.

**Table 8. Effect of the Acidic/Basic Site Ratio on the Initial Production Rate and Content at Equilibrium of FAMEs**[a]

| catalyst | total acidic sites/total basic sites | initial FAME production rate | FAME content at equilibrium |
|---|---|---|---|
| Cat_1 | 3.41 | 29 | 91% |
| Cat_2 | 5.46 | 88 | 90% |

[a]Reaction conditions: $T$ = 60 °C, methanol/oil molar ratio = 12, $W_{cat}$ = 5 wt %

Cat_2 ($4.6 USD/g) is about 6.5 times higher than Cat_1 ($0.70 USD/g).

*3.2.3. Effect of Fe Content and the Plausible Reaction Pathway on the Synthesized Catalysts.* In order to investigate the influence of the iron content in the prepared catalysts, different percentages of iron related to the catalyst weight were tested: 0, 1, 2.5, 5, and 10 wt % for every proposed material. The results shown in Figure 8 indicate that the higher the percentage of iron, the greater the FAME content obtained. Thus, when 10 wt % of iron was incorporated, the maximum FAME content was obtained, that is, 91 and 90% at equilibrium for Cat_1 and Cat_2, respectively. Given the instrumental error, this difference is not considered significant. Interestingly enough, the trend observed with the catalysts with lower content than 10 wt %, is rather different, mainly for Cat_1. It can be observed in Figure 8 that for the catalysts with an Fe wt % between 1 and 5, the FAME content reaches a maximum after 2 h of reaction and then steeply decreases without achieving an equilibrium state. This equilibrium state refers to the transesterification reaction indicated in Schemes 1a, 2a, and 3 and is achieved when both rates are equalized, that is, the one to produce the esters and the one to reconvert them into mono-, di-, and triglycerides. It is worth pointing out that the rate at which the FAME content decreases is inversely proportional to the amount of added iron, and then, the final

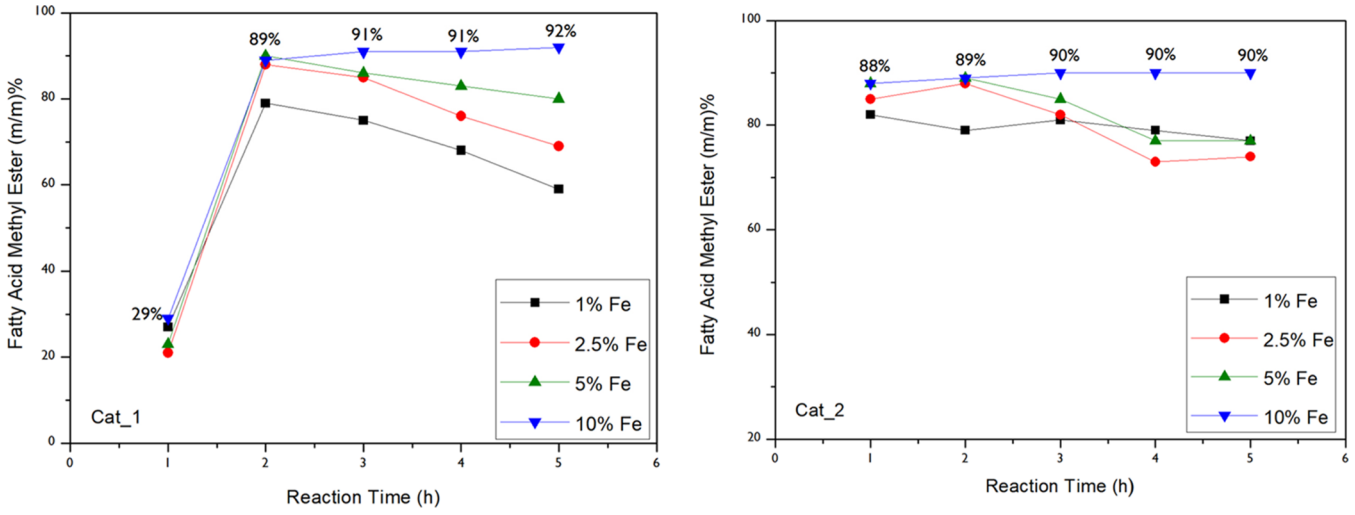


**Figure 8.** Effect of Fe wt % over CaO on FAME profiles as a function of time for Cat_1 and Cat_2 catalysts. Reaction conditions: $T$ = 60 C, 12:1 methanol/oil molar ratio, $W_{cat}$ = 5 wt %.



https://doi.org/10.1021/acsomega.1c03586
ACS Omega 2021, 6, 24092−24105

**Scheme 1. FAME Consumption Routes as a Function of Iron Concentration: (a) High Iron Content and (b) Low Iron Content**

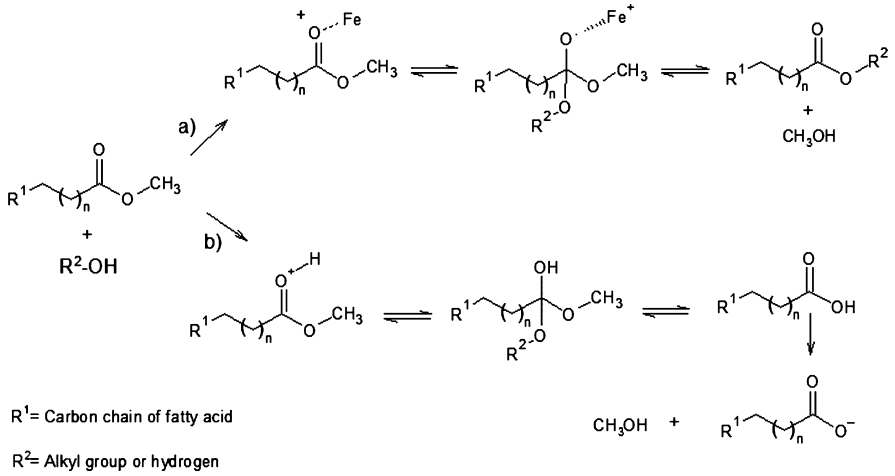


**Scheme 2. (a) Base-Catalyzed Reaction Pathway for Ester Production from Triglycerides (Adapted from Lamb et al.[7]); (b) Acid-Catalyzed Esterification of FFA (Adapted from Wan Omar et al.[34])**

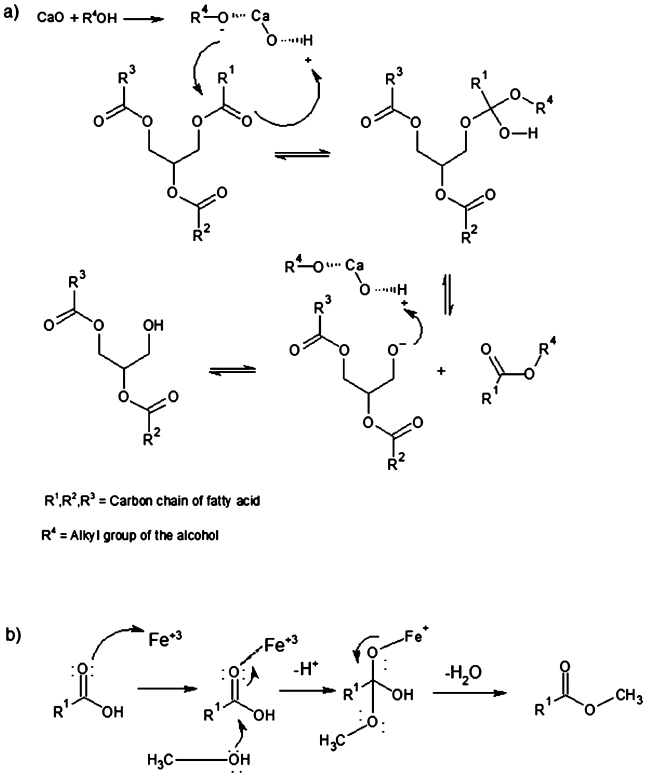


FAME content, after 5 h of reaction, keeps a direct relationship with the iron content. This trend can be explained based on the plausible reactions of the produced FAMEs according to Scheme 1. It is proposed here that when the iron content increases, route (a) is favored, thus maintaining the equilibrium observed with the catalyst with the highest iron content (see Figure 8). FAMEs, however, can also be hydrolyzed by route (b) in Scheme 1. In such a case, the products are fatty acids and saponification products. For route (b) to proceed, the chemical substituent $R^2$ should be hydrogen, and therefore, this route will be favored under both, low iron content in the catalyst and the presence of water. This water can be part of the initial composition of the feedstock or being produced during the esterification step (Scheme 2b). This concurs with our observation during experimentation since a fatty and sticky solid was obtained when the catalyst with the lowest iron content was utilized. In addition, in the cases where a maximum of FAMEs is reached but equilibrium is not (catalysts with iron content lower than 10%), the reaction to the left in Schemes 2a and 3 is also favored. At this point, it is worth noticing that within the time before a maximum of the FAME content is reached (2 h for Cat_1 and 1 h for Cat_2), the transesterification rate in Schemes 2a and 3 (to the right) is faster than the corresponding reversible rate.

Besides favoring route (a) in Scheme 1, the role of iron ions in the resulting mixed oxide is to provide acidic sites necessary for the esterification of FFAs. When using only CaO (0% iron), a 49% FAME was obtained after 2 h of reaction, and in the third hour, the mixture became a solid fat. This can be ascribed to the high content of FFAs (1.26 wt %) in the WCO, favoring saponification.[45,47] The low FAME content achieved was expected since, according to several authors, the basic catalysts have a better catalytic activity, in the transesterification reaction, if feedstock with less than 1 wt % FFA is used.[48] The saponification is evidence of the combination of the FFA with the basic sites, and water is also produced in this step.[6] Nevertheless, the WCOs also have triglycerides (see Table 2), and these are the main source of the obtained FAMEs when using only CaO. For this reaction to proceed, methanol must be first chemisorbed, so when triglycerides reach the surface, they can react with the chemisorbed methoxy group (Scheme 2a).[7] According to Scheme 2a, esters are the product of this reaction, and a diglyceride is produced and follows the same reaction as triglycerides. This is repeated 3 times until 3 mol of esters and 1 mol of glycerol are produced per mole of triglycerides.

By contrasting the results obtained with CaO (49% FAMEs after 2 h) and with the iron- and calcium-based catalysts (Figure 8), the advantage of adding iron is evident and implies an increase in the acidic-site density necessary to conduct the esterification reaction of the FFA. The mechanism of this process has been previously reported and is depicted by Scheme 2b.[8] It consists of three main steps: (i) chemisorption of the FFA on an acidic site (iron ions in this case), (ii)


https://doi.org/10.1021/acsomega.1c03586
ACS Omega 2021, 6, 24092−24105

Scheme 3. Transesterification on Acidic Sites (Adapted from Lotero et al.[49])

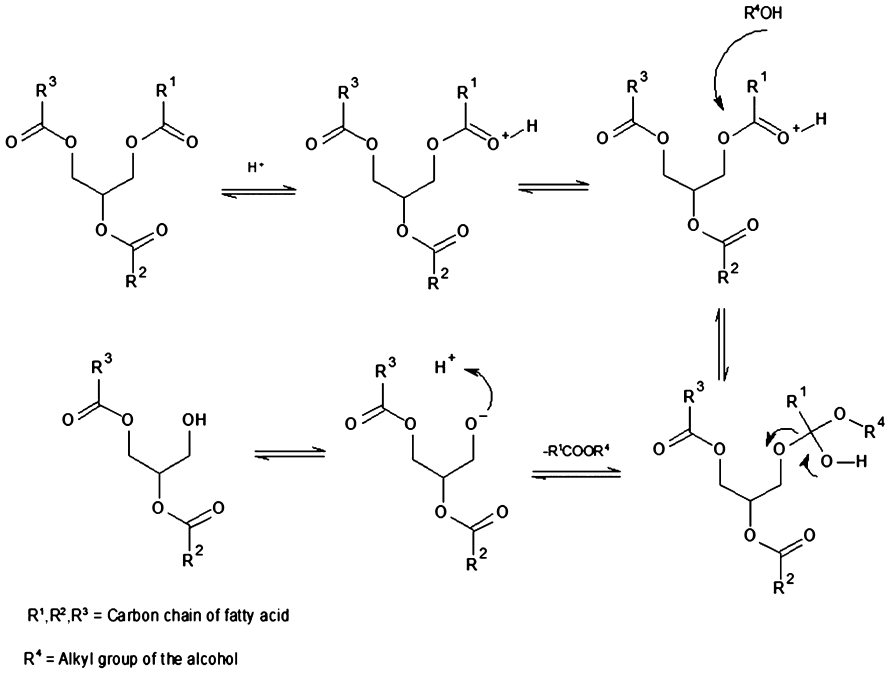


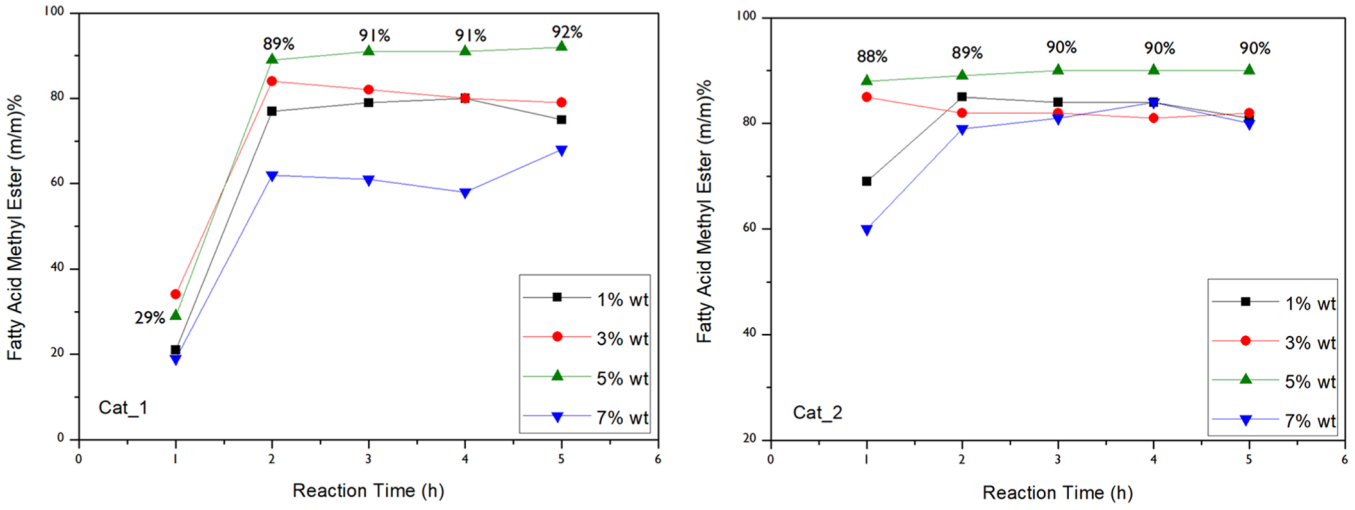


Figure 9. Effect of catalyst loading on FAME profiles as a function of time for Cat_1 and Cat_2 catalysts. Reaction conditions: $T$ = 60 C, methanol/oil molar ratio: 12:1 and 10 wt % of iron.

reaction of bulk methanol with chemisorbed FFA, and (iii) desorption of the methyl ester and water.

Transesterification can also occur on acidic sites by means of the reaction depicted in Scheme 3.[49] These sites can be any proton donors such as $H^+$ or iron ions. This process, however, is expected to proceed at a much lower rate than that in Scheme 2.

In summary, the role of iron in the prepared catalysts is to provide acidic sites to esterify the FFA in the WCO and transesterify triglycerides.

Because of the aforesaid, the global reaction pathway with the prepared catalysts is obtained when Schemes 1−3 are placed together.

*3.2.4. Effect of Catalyst Loading ($W_{cat}$).* Catalyst loading is an important variable that affects biodiesel production since it is intimately related to both external and internal mass transfer resistances.[50] When the process is free of mass transfer resistances or these are minimized, the FAME content is expected to increase when catalyst loading increases; however, there is a maximum increase and therefore, it is necessary to identify the appropriate amount of the catalyst that provides the active sites to carry out the biodiesel production because exceeding the optimal amount dramatically reduces performance. For this reason, this variable needs proper control.

As can be seen in Figure 9, both catalysts exhibit a similar performance for the same catalyst loading, except for 7% wt. The produced FAMEs were less when 1 and 3% of catalyst loadings were used and increased when the amount of the catalyst increased to 5%. Nevertheless, it was observed that by increasing the amount of the catalyst to 7%, the FAMEs obtained considerably decreased; this effect can be attributed to two important reasons: (1) a greater amount of the catalyst causes an increase in viscosity, favoring resistance to mass transfer,[1,50,51] and (2) the agglomeration of the catalyst within


https://doi.org/10.1021/acsomega.1c03586
ACS Omega 2021, 6, 24092−24105

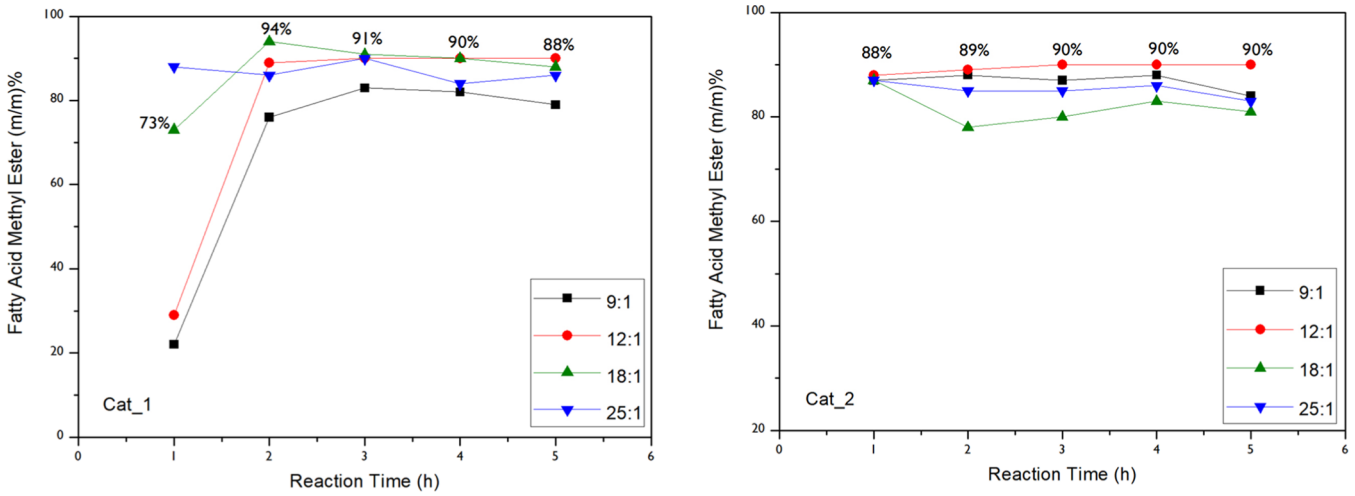


**Figure 10.** Effect of methanol/oil ratio on FAME profiles as a function of time for Cat_1 and Cat_2 catalysts. Reaction conditions: 60 °C, 5 h, and 5 wt % of the catalyst.

the reaction system, which was observed during the reaction, causes a decrease in the available active surface area, diffusion, and mixing problems.[1,52] Because of the aforementioned reasons, 5 wt % of catalyst loading was selected as the optimum.

*3.2.5. Effect of Methanol/Oil Molar Ratio.* The alcohol/oil molar ratio is one of the most relevant parameters during the optimization of biodiesel production due to being closely related to production costs. Since biodiesel production is a reversible process, an extra amount of alcohol is required to force the process to the right side of the products.[44] In this work, an excess of methanol was used to obtain a higher FAME content in the produced biodiesel.

The effect of methanol/WCO molar ratio on the FAME content is shown in Figure 10. The FAME temporary profile for Cat_1 indicated that when the molar ratio was increased from 9:1 to 18:1, the FAME content increased from 83 to 91%, respectively, in the third hour of the reaction. However, when the molar ratio was increased to 25:1, the FAME content decreases and 90% of FAMEs were obtained in the third reaction hour. This trend was consistent with that previously obtained by Ezzah-Mahmudah et al.,[1] who reported the reduction of FAME content when methanol exceeded its optimum amount due to the moisture inside the methanol solution, causing the hydrolysis of the FAMEs (see Scheme 1b). Moreover, the separation of methyl esters and glycerol from the reaction mixture becomes difficult due to the polar hydroxyl group derived from methanol acting as the emulsifier.[53]

For the Cat_2 catalyst, a similar trend was observed when the methanol/oil molar ratio was increased from 9:1 to 12:1, and the FAME content of biodiesel increased from 87 to 90% in the third hour. Higher addition of methanol to the reaction mixture resulted in reduction of FAMEs. Hence, in this work, a methanol/oil molar ratio of 12:1 was considered as the optimal ratio.

In addition, in contrast to the results obtained with Cat_1 and Cat_2, as depicted in Figure 10, it is worth noticing that despite having the same active phases, the effect of the alcohol/oil molar ratio on the initial production rate of FAMEs is different. For Cat_1, this rate increases when increasing the alcohol/oil molar ratio, while for Cat_2, this rate does not show a correlation with the alcohol/oil molar ratio. Since these catalysts are also similar in morphology, these results suggest that the effect of the alcohol/oil molar ratio depends, once again, on the ratio of acidic/basic sites (see Table 8). A higher ratio (Cat 2) demands a lower methanol/oil ratio to achieve the maximum FAME % at a higher initial rate than when the ratio of the acidic/basic sites is lower, which is the case for Cat_1, despite exhibiting a higher number of acidic and basic sites with higher strength than Cat_ 2. This can be ascribed to methanol being highly consumed, as expected, by the high number of basic sites in Cat_1. This might lead to methanol deprivation for the acidic sites. In consequence, the methyl ester initial production rate from the FFAs in the waste oil is significantly lower when compared to that obtained with Cat_2 at the same methanol/oil molar ratio (see Table 8). Thus, to achieve the same initial rate with Cat_1 as with Cat_2, the methanol/oil molar ratio should be about twice (25:1 instead of 12:1). This molar ratio allows having enough available methanol to occupy the basic sites and also to react with the expected FFAs chemisorbed onto the acidic sites, according to the mechanism suggested by Wan Omar et al.[34] (see Scheme 2b). Therefore, these results suggest that the ratio of acidic/basic sites is an important parameter at the time of minimizing the required alcohol/oil molar ratio.

Finally, it is worth noticing that for both catalysts, once equilibrium is reached with all the assessed molar ratios (after 2 h for Cat_1 and after 1 h for Cat_2), there is not an appreciable effect on the FAME content for molar ratios higher than 9:1 for Cat_1 and for all molar ratios for Cat_2, except at 18:1. Therefore, despite the initial production rates being different for Cat_1, at the end, the selection of the methanol/oil molar ratio can be done based on the overall cost.

It is important to highlight that the optimum alcohol/oil molar ratio reported in previous studies for bifunctional catalysis (under similar reaction conditions) is greater than that obtained in this work to achieve similar percentages of FAME content in biodiesel; for example, the catalyst of cesium and zirconium doped in alumina ($Cs-Zr/Al_2O_3$) required an optimum alcohol/oil ratio of 20:1 to reach 90% of FAMEs;[54] 92.1% of FAMEs was reached using a sulfated iron catalyst ($Fe_2O_3/SO_4^{-2}$) and an alcohol/oil ratio of 25:1;[46] an alcohol/oil ratio of 20:1 led to obtain 94.3% FAMEs with the CaO/


https://doi.org/10.1021/acsomega.1c03586
ACS Omega 2021, 6, 24092−24105

$La_2O_3$ catalyst.[55] In the case of CaO doped with iron oxides and high-FFA-content oil, the optimum value reported for the alcohol/oil molar ratio was 15:1 reported by Ezzah-Mahmudah et al.[1] and 10:1 by Helwani et al.[24] It is worth pointing out that in both cases, the reaction temperature was higher, that is, 65 and 70 °C, respectively, than the one used in this study (60 °C).

*3.2.6. Effect of Reaction Time.* The effect of reaction time was studied by employing optimal reaction conditions: methanol/oil ratio 12:1, 5 wt % of catalyst at 60 °C, and atmospheric pressure. The reaction was monitored for 5 h. As can be seen in Figure 7, equilibrium is reached using both proposed bifunctional catalysts, Cat_1 and Cat_2, within the first 2 h of the reaction considering that there is an error of 2%. The FAME % decreases slightly during the following hours; this can be attributed to the reversibility of the process, and this has also been previously observed by other researchers.[39,46] For this reason, 1 h was established as the optimal time to reach the maximum performance with Cat_2 and 2 h for Cat_1.

**3.3. Reusability Test of the Catalyst.** The stability of the catalytic activity of the Cat_2 catalyst was evaluated by determining the reusability, which is an important factor for heterogeneous catalysts due to their production cost.[31,54]

Reusability was determined by analyzing the amount of FAMEs that the catalyst is able to produce during consecutive reaction cycles. All experiments were performed under the previously determined optimal reaction conditions (temperature 60 °C, 5 wt % catalyst, and 10 wt % of Fe over CaO using iron(III) nitrate as the precursor). After 3 hours of the reaction, the components of the mixture (methanol, FAMEs, glycerol, and catalyst) were separated, a sample of FAMEs was taken, and the catalyst was recovered and washed with methanol and hexane for the subsequent use in a new reaction. In the first reaction, 90% of FAMEs was reached; in the second reaction, 88%, and during the third cycle, an 89% of FAMEs was obtained. According to the implicit error, this is not considered to be a significant difference and therefore, Cat_2 can be used up to 3 times without compromising its catalytic activity.

**3.4. Characterization of the Synthesized Biodiesel.** Table 9 shows some properties of biodiesel obtained under optimal reaction conditions; $Fe(NO_3)_3{\cdot}9H_2O$ over CaO, alcohol/oil ratio 12:1, temperature 60 °C, 5% of the catalyst, and 10% by weight of iron over CaO. The amount of FAMEs, density at 15 °C, and kinematic viscosity at 40 °C were determined according to the European Union Quality Standard (EN-14214). It is worth pointing out that these parameters comply with the aforementioned standard.

**Table 9. Characterization of Biodiesel**

| property | value |
|---|---|
| FAMEs | 91% |
| free fatty acid (wt %) | 0.27 |
| density at 15 °C | 894.46 kg/m$^3$ |
| viscosity at 40 °C | 4.6 mm$^2$/s |

## 4. CONCLUSIONS

In this work, two bifunctional catalysts were prepared and tested in the conversion of WCO with high content of FFAs, into biodiesel. The active phases of such catalysts are CaO, $Ca_2Fe_2O_5$, and $CaFeO_3$. $Fe_2O_3$ was not found in the catalyst. The addition of the iron phases allows attaining a FAME content of 90%, while with the use of CaO, only 49% is reached. The results suggest that what dictates the methanol/oil molar ratio and the initial FAME production rate is not the total amount and strength of acidic and basic sites but the ratio of them. A way to vary this ratio is by changing the iron precursor. The use of $Fe_2O_3$ as a precursor leads to a higher density of basic and acidic sites; however, when using $Fe(NO_3)_3{\cdot}9H_2O$, the ratio of acidic to basic sites is almost double than that obtained with the oxide. This leads to reach equilibrium at half of the time used with the catalyst prepared with the other precursor ($Fe_2O_3$). Nevertheless, the production cost of the catalyst prepared with $Fe(NO_3)_3{\cdot}9H_2O$ is 6.5 times higher than the catalyst prepared with $Fe_2O_3$.

Finally, it can be concluded that the prepared catalyst using the salt as the precursor (Cat_2) has the potential to catalyze esterification and transesterification simultaneously under mild conditions. The obtained FAME percentage with this catalyst was 90% at optimum reaction conditions of: 10 wt % of iron over CaO, methanol/oil ratio 12:1, 5 wt % of the catalyst, temperature of the reaction 60 °C, atmospheric pressure, and 1 h of reaction time. At the best reaction conditions with both catalysts, there were not observed problems of emulsification or saponification. The latter was observed when using undoped CaO and with Cat_1 with low iron content. The synthesized catalyst was easily recovered and was capable of being reused at least 3 times.

## AUTHOR INFORMATION


### Corresponding Authors

**Rubi Romero** − *Chemical Engineering Lab., Centro Conjunto de Investigación en Química Sustentable, UAEM-UNAM, Universidad Autónoma del Estado de México, Toluca 50200, Mexico;* orcid.org/0000-0001-9163-7936; Email: rromeror@uaemex.mx

**Reyna Natividad** − *Chemical Engineering Lab., Centro Conjunto de Investigación en Química Sustentable, UAEM-UNAM, Universidad Autónoma del Estado de México, Toluca 50200, Mexico;* orcid.org/0000-0001-8978-1066; Email: rnatividadr@uaemex.mx

### Authors

**Vania Enguilo Gonzaga** − *Chemical Engineering Lab., Centro Conjunto de Investigación en Química Sustentable, UAEM-UNAM, Universidad Autónoma del Estado de México, Toluca 50200, Mexico*

**Rosa María Gómez-Espinosa** − *Chemical Engineering Lab., Centro Conjunto de Investigación en Química Sustentable, UAEM-UNAM, Universidad Autónoma del Estado de México, Toluca 50200, Mexico*

**Amaya Romero** − *Chemical Engineering Department, University of Castilla-La Mancha, Ciudad Real 13071, Spain*

**Sandra Luz Martínez** − *Faculty of Chemistry, Universidad Autónoma del Estado de México, Toluca 50120 Estado de México, Mexico*

Complete contact information is available at: https://pubs.acs.org/10.1021/acsomega.1c03586


### Notes

The authors declare no competing financial interest.



https://doi.org/10.1021/acsomega.1c03586
ACS Omega 2021, 6, 24092−24105

## ■ ACKNOWLEDGMENTS

The authors are grateful for the technical support by Dr. Susana Hernández López from Facultad de Química UAEM and Dr. Uvaldo Hernández Balderas and Citlalit Martínez Soto from Centro Conjunto de Investigación en Química Sustentable UAEM-UNAM. The financial support of Universidad Autónoma del Estado de México through Project 5021/2020/CIB is also acknowledged. V.E.G. wishes to thank Consejo Nacional de Ciencia y Tecnología (CONACYT) for scholarship no. 861011 to conduct postgraduate studies. CONACYT is also acknowledged for project 269093.

## ■ REFERENCES

(1) Ezzah-Mahmudah, S.; Lokman, I. M.; Saiman, M. I.; Taufiq-Yap, Y. H. Synthesis and Characterization of Fe2O3/CaO Derived from Anadara Granosa for Methyl Ester Production. *Energy Convers. Manage.* **2016**, *126*, 124−131.

(2) Mueanmas, C.; Nikhom, R.; Petchkaew, A.; Iewkittayakorn, J.; Prasertsit, K. Extraction and Esterification of Waste Coffee Grounds Oil as Non-Edible Feedstock for Biodiesel Production. *Renewable Energy* **2019**, *133*, 1414−1425.

(3) Bacovsky, D.; Ludwiczek, N.; Pointner, C.; Verma, V. K. *IEA Bioenergy Countries' Report: Bioenergy Policies and Status of Implementation*, 2016, p 120.

(4) Farooq, M.; Ramli, A.; Subbarao, D. Biodiesel Production from Waste Cooking Oil Using Bifunctional Heterogeneous Solid Catalysts. *J. Cleaner Prod.* **2013**, *59*, 131−140.

(5) Vujicic, D.; Comic, D.; Zarubica, a.; Micic, R.; Boskovic, G. Kinetics of Biodiesel Synthesis from Sunflower Oil over CaO Heterogeneous Catalyst. *Fuel* **2010**, *89*, 2054−2061.

(6) Xie, W.; Zhao, L. Production of Biodiesel by Transesterification of Soybean Oil Using Calcium Supported Tin Oxides as Heterogeneous Catalysts. *Energy Convers. Manage.* **2013**, *76*, 55−62.

(7) Lam, M. K.; Lee, K. T.; Mohamed, A. R. Homogeneous, Heterogeneous and Enzymatic Catalysis for Transesterification of High Free Fatty Acid Oil (Waste Cooking Oil) to Biodiesel: A Review. *Biotechnol. Adv.* **2010**, *28*, 500−518.

(8) Talebian-Kiakalaieh, A.; Amin, N. A. S.; Mazaheri, H. A Review on Novel Processes of Biodiesel Production from Waste Cooking Oil. *Appl. Energy* **2013**, *104*, 683−710.

(9) Zhang, H.; Li, H.; Hu, Y.; Venkateswara Rao, K. T.; Xu Charles, C.; Yang, S. Advances in Production of Bio-Based Ester Fuels with Heterogeneous Bifunctional Catalysts. *Renewable Sustainable Energy Rev.* **2019**, *114*, 109296.

(10) Al-Saadi, A.; Mathan, B.; He, Y. Esterification and transesterification over SrO-ZnO/Al2O3 as a novel bifunctional catalyst for biodiesel production. *Renewable Energy* **2020**, *158*, 388−399.

(11) Liu, Y.; Zhang, P.; Fan, M.; Jiang, P. Biodiesel production from soybean oil catalyzed by magnetic nanoparticle MgFe 2 O 4 @CaO. *Fuel* **2016**, *164*, 314−321.

(12) Rahimi, T.; Kahrizi, D.; Feyzi, M.; Ahmadvandi, H. R.; Mostafaei, M. Catalytic performance of MgO /Fe2O3-SiO2 core-shell magnetic nanocatalyst for biodiesel production of Camelina sativa seed oil: Optimization by RSM-CCD method. *Ind. Crops Prod.* **2021**, *159*, 113065.

(13) Mokhatr Mohamed, M.; El-Faramawy, H. An innovative nanocatalyst $\alpha$-Fe2O3/AlOOH processed from gibbsite rubbish ore for efficient biodiesel production via utilizing cottonseed waste oil. *Fuel* **2021**, *297*, 120741.

(14) Mohamed, M. M.; Bayoumy, W. A.; El-Faramawy, H.; El-Dogdog, W.; Mohamed, A. A. A novel $\alpha$-Fe2O3/AlOOH($\gamma$-Al2O3) nanocatalyst for efficient biodiesel production from waste oil: Kinetic and thermal studies. *Renewable Energy* **2020**, *160*, 450−464.

(15) Teo, S. H.; Islam, A.; Chan, E. S.; Thomas Choong, S. Y.; Alharthi, N. H.; Taufiq-Yap, Y. H.; Awual, M. R. Efficient Biodiesel Production from Jatropha Curcus Using CaSO4/Fe2O3-SiO2 Core-Shell Magnetic Nanoparticles. *J. Cleaner Prod.* **2019**, *208*, 816−826.

(16) Chiang, C.-L.; Lin, K.-S.; Shu, C.-W.; Wu, J. C.-S.; Wu, K. C.-W.; Huang, Y.-T. Enhancement of Biodiesel Production via Sequential Esterification/Transesterification over Solid Superacidic and Superbasic Catalysts. *Catal. Today* **2020**, *348*, 257−269.

(17) Lee, H. V.; Juan, J. C.; Taufiq-Yap, Y. H. Preparation and application of binary acid-base CaO-La 2 O 3 catalyst for biodiesel production. *Renewable Energy* **2015**, *74*, 124−132.

(18) Syazwani, O. N.; Rashid, U.; Mastuli, M. S.; Taufiq-Yap, Y. H. Esterification of Palm Fatty Acid Distillate (PFAD) to Biodiesel Using Bi-Functional Catalyst Synthesized from Waste Angel Wing Shell (Cyrtopleura Costata). *Renewable Energy* **2019**, *131*, 187−196.

(19) Marinković, D. M.; Miladinović, M. R.; Avramović, J. M.; Krstić, I. B.; Stanković, M. V.; Stamenković, O. S.; Jovanović, D. M.; Veljković, V. B. Kinetic modeling and optimization of sunflower oil methanolysis catalyzed by spherically-shaped CaO/$\gamma$-Al2O3 catalyst. *Energy Convers. Manage.* **2018**, *163*, 122−133.

(20) Mansir, N.; Teo, S. H.; Mijan, N.-A.; Taufiq-Yap, Y. H. Efficient Reaction for Biodiesel Manufacturing Using Bi-Functional Oxide Catalyst. *Catal. Commun.* **2021**, *149*, 106201.

(21) Xue, B.-j.; Luo, J.; Zhang, F.; Fang, Z. Biodiesel production from soybean and Jatropha oils by magnetic CaFe2O4-Ca2Fe2O5-based catalyst. *Energy* **2014**, *68*, 584−591.

(22) Khandan, M.; Saffarzadeh-Matin, S.; shalmashi, A. Green Hydrophobization of Fume Silica: Tailoring of Heterogeneous Basic Catalyst for Biodiesel Production. *J. Cleaner Prod.* **2020**, *260*, 121066.

(23) Mansir, N.; Teo, S. H.; Rabiu, I.; Taufiq-Yap, Y. H. Effective Biodiesel Synthesis from Waste Cooking Oil and Biomass Residue Solid Green Catalyst. *Chem. Eng. J.* **2018**, *347*, 137−144.

(24) Helwani, Z.; Ramli, M.; Saputra, E.; Bahruddin, B.; Yolanda, D.; Fatra, W.; Idroes, G. M.; Muslem, M.; Mahlia, T. M. I.; Idroes, R. Impregnation of CaO from Eggshell Waste with Magnetite as a Solid Catalyst (Fe3O4/CaO) for Transesterification of Palm Oil off-Grade. *Catalysts* **2020**, *10*, 164.

(25) Helmiyati, H.; Masriah, I. Preparation of Cellulose/CaO-Fe2O3 Nanocomposites as Catalyst for Fatty Acid Methyl Ester Production. *AIP Conf. Proc.* **2019**, *2168*, 020062.

(26) Mansir, N.; Teo, S. H.; Rashid, U.; Taufiq-Yap, Y. H. Efficient Waste Gallus Domesticus Shell Derived Calcium-Based Catalyst for Biodiesel Production. *Fuel* **2018**, *211*, 67−75.

(27) Shi, M.; Zhang, P.; Fan, M.; Jiang, P.; Dong, Y. Influence of Crystal of Fe2O3 in Magnetism and Activity of Nanoparticle CaO@Fe2O3 for Biodiesel Production. *Fuel* **2017**, *197*, 343−347.

(28) Camacho, J. N.; Natividad, R.; Galvan Muciño, G. E.; García-Orozco, I.; Baeza, R.; Romero, R. Comparative Study of Quick Lime and CaO as Catalysts of Safflower Oil Transesterification. *Int. J. Chem. React. Eng.* **2016**, *14*, 909−917.

(29) Nunes, A. L. B.; Castilhos, F. Chemical Interesterification of Soybean Oil and Methyl Acetate to FAME Using CaO as Catalyst. *Fuel* **2020**, *267*, 117264.

(30) Di Felice, L.; Courson, C.; Niznansky, D.; Foscolo, P. U.; Kiennemann, A. Biomass Gasification with Catalytic Tar Reforming: A Model Study into Activity Enhancement of Calcium- and Magnesium-Oxide-Based Catalytic Materials by Incorporation of Iron. *Energy Fuels* **2010**, *24*, 4034−4045.

(31) Alhassan, F. H.; Rashid, U.; Taufiq-Yap, Y. H. Synthesis of waste cooking oil-based biodiesel via effectual recyclable bi-functional Fe2O3MnOSO42−/ZrO2 nanoparticle solid catalyst. *Fuel* **2015**, *142*, 38−45.

(32) Miladinović, M. R.; Krstić, J. B.; Tasić, M. B.; Stamenković, O. S.; Veljković, V. B. A Kinetic Study of Quicklime-Catalyzed Sunflower Oil Methanolysis. *Chem. Eng. Res. Des.* **2014**, *92*, 1740−1752.

(33) Rabiah Nizah, M. F.; Taufiq-Yap, Y. H.; Rashid, U.; Teo, S. H.; Shajaratun Nur, Z. A.; Islam, A. Production of biodiesel from non-edible Jatropha curcas oil via transesterification using Bi 2 O 3 -La 2 O 3 catalyst. *Energy Convers. Manage.* **2014**, *88*, 1257−1262.

(34) Wan Omar, W. N. N.; Amin, N. A. S. Biodiesel Production from Waste Cooking Oil over Alkaline Modified Zirconia Catalyst. *Fuel Process. Technol.* **2011**, *92*, 2397−2405.



https://doi.org/10.1021/acsomega.1c03586
*ACS Omega* 2021, 6, 24092−24105

(35) Zamboni, I.; Courson, C.; Kiennemann, A. Synthesis of Fe/CaO Active Sorbent for CO2 Absorption and Tars Removal in Biomass Gasification. *Catal. Today* **2011**, *176*, 197−201.
(36) Boro, J.; Konwar, L. J.; Thakur, A. J.; Deka, D. Ba doped CaO derived from waste shells of T striatula (TS-CaO) as heterogeneous catalyst for biodiesel production. *Fuel* **2014**, *129*, 182−187.
(37) Jeon, J.-W.; Jung, S.-M.; Sasaki, Y. Formation of Calcium Ferrites under Controlled Oxygen Potentials at 1273 K. *ISIJ Int.* **2010**, *50*, 1064−1070.
(38) Wieczorek-Ciurowa, K.; Kozak, A. J. The Thermal Decomposition of Fe(NO3)3·9H2O. *J. Therm. Anal. Calorim.* **1999**, *58*, 647−651.
(39) Faraldos, M. *GobernaTécnicas de AnálisisCaracterización de Materiales, C. y Consejo Superior de Investigaciones Científicas*: Madrid, 2011.
(40) Sun, Z.; Chen, S.; Russell, C. K.; Hu, J.; Rony, A. H.; Tan, G.; Chen, A.; Duan, L.; Boman, J.; Tang, J.; Chien, T.; Fan, M.; Xiang, W. Improvement of H2-Rich Gas Production with Tar Abatement from Pine Wood Conversion over Bi-Functional Ca2Fe2O5 Catalyst: Investigation of Inner-Looping Redox Reaction and Promoting Mechanisms. *Appl. Energy* **2018**, *212*, 931−943.
(41) Meher, L. C.; Kulkarni, M. G.; Dalai, A. K.; Naik, S. N. Transesterification of karanja(Pongamia pinnata) oil by solid basic catalysts. *Eur. J. Lipid Sci. Technol.* **2006**, *108*, 389−397.
(42) Molaei Dehkordi, A.; Ghasemi, M. Transesterification of Waste Cooking Oil to Biodiesel Using Ca and Zr Mixed Oxides as Heterogeneous Base Catalysts. *Fuel Process. Technol.* **2012**, *97*, 45−51.
(43) Pasupulety, N.; Gunda, K.; Liu, Y.; Rempel, G. L.; Ng, F. T. T. Production of Biodiesel from Soybean Oil on CaO/Al2O3 Solid Base Catalysts. *Appl. Catal., A* **2013**, *452*, 189−202.
(44) Alhassan, F. H.; Rashid, U.; Taufiq-Yap, Y. H. Synthesis of Waste Cooking Oil Based Biodiesel via Ferric-Manganese Promoted Molybdenum Oxide / Zirconia Nanoparticle Solid acid Catalyst: Influence of Ferric and Manganese Dopants. *J. Oleo Sci.* **2015**, *64*, 505−514.
(45) Muciño, G. G.; Romero, R.; Ramírez, A.; Martínez, S. L.; Baeza-Jiménez, R.; Natividad, R. Biodiesel Production from Used Cooking Oil and Sea Sand as Heterogeneous Catalyst. *Fuel* **2014**, *138*, 143−148.
(46) Zhai, D.; Nie, Y.; Yue, Y.; He, H.; Hua, W.; Gao, Z. Esterification and Transesterification on Fe2O3-Doped Sulfated Tin Oxide Catalysts. *Catal. Commun.* **2011**, *12*, 593−596.
(47) Demirbas, A. Biodiesel from Waste Cooking Oil via Base-Catalytic and Supercritical Methanol Transesterification. *Energy Convers. Manage.* **2009**, *50*, 923−927.
(48) Freedman, B.; Pryde, E. H.; Mounts, M. T. Variables Affecting the Yield of Fatty Esters from Transesterification Vegetable Oils. *J. Am. Oil Chem. Soc.* **1984**, *61*, 1638−1643.
(49) Lotero, E.; Liu, Y.; Lopez, D. E.; Suwannakarn, K.; Bruce, D. A.; Goodwin, J. G. Synthesis of Biodiesel via Acid Catalysis. *Ind. Eng. Chem. Res.* **2005**, *44*, 5353−5363.
(50) Yan, S.; Lu, H.; Liang, B. Supported CaO Catalysts Used in the Transesterification of Rapeseed Oil for the Purpose of Biodiesel Production. *Energy Fuels* **2007**, *22*, 646−651.
(51) Hindryawati, N.; Maniam, G. P.; Karim, M. R.; Chong, K. F. Transesterification of Used Cooking Oil over Alkali Metal (Li, Na, K) Supported Rice Husk Silica as Potential Solid Base Catalyst. *Eng. Sci. Technol.* **2014**, *17*, 95−103.
(52) Asri, N. P.; Machmudah, S.; Wahyudiono; Suprapto; Budikarjono, K.; Roesyadi, A.; Goto, M. Palm Oil Transesterification in Sub- and Supercritical Methanol with Heterogeneous Base Catalyst. *Chem. Eng. Process.* **2013**, *72*, 63−67.
(53) Liu, X.; He, H.; Wang, Y.; Zhu, S. Transesterification of Soybean Oil to Biodiesel Using SrO as a Solid Base Catalyst. *Catal. Commun.* **2007**, *8*, 1107−1111.
(54) Amani, H.; Ahmad, Z.; Hameed, B. H. Highly Active Alumina-Supported Cs−Zr Mixed Oxide Catalysts for Low-Temperature Transesterification of Waste Cooking Oil. *Appl. Catal., A* **2014**, *487*, 16−25.
(55) Yan, S.; Kim, M.; Salley, S. O.; Ng, K. Y. S. Oil Transesterification over Calcium Oxides Modified with Lanthanum. *Appl. Catal., A* **2009**, *360*, 163−170.


https://doi.org/10.1021/acsomega.1c03586
*ACS Omega* 2021, 6, 24092−24105